A fast approach to refraction-aware eye-model fitting and gaze prediction

Kai Dierkes
Pupil Labs Research, Berlin
kai@pupil-labs.com

Moritz Kassner
Pupil Labs Research, Berlin
moritz@pupil-labs.com

Andreas Bulling
Pupil Labs Research, Berlin
andreas@pupil-labs.com

ABSTRACT

By temporally integrating information about pupil contours extracted from eye images, model-based methods for glint-free gaze estimation can mitigate pupil detection noise. However, current approaches require time-consuming iterative solving of a nonlinear minimization problem to estimate key parameters, such as eyeball position. Based on the method presented by [Swirski and Dodgson 2013], we propose a novel approach to glint-free 3D eye-model fitting and gaze prediction using a single near-eye camera. By recasting model optimization as a least-squares intersection of lines, we make it amenable to a fast non-iterative solution. We further present a method for estimating deterministic refraction-correction functions from synthetic eye images and validate them on both synthetic and real eye images. We demonstrate the robustness of our method in the presence of pupil detection noise and show the benefit of temporal integration of pupil contour information on eyeball position and gaze estimation accuracy.

CCS CONCEPTS

• **Computing methodologies → Computer vision**;
Model development and analysis; *Tracking*.

KEYWORDS

Eye tracking, refraction, 3D eye model, pupil detection, contour-based, glint-free

1 INTRODUCTION

Over the last decades, camera-based eye trackers have become a potent and wide-spread research tool in fields as disparate as market research, psychology, and human-computer interaction. Offering increased mobility compared to remote eye-tracking solutions, head-mounted eye trackers, in particular, have enabled the acquisition of gaze data during dynamic activities also in outdoor
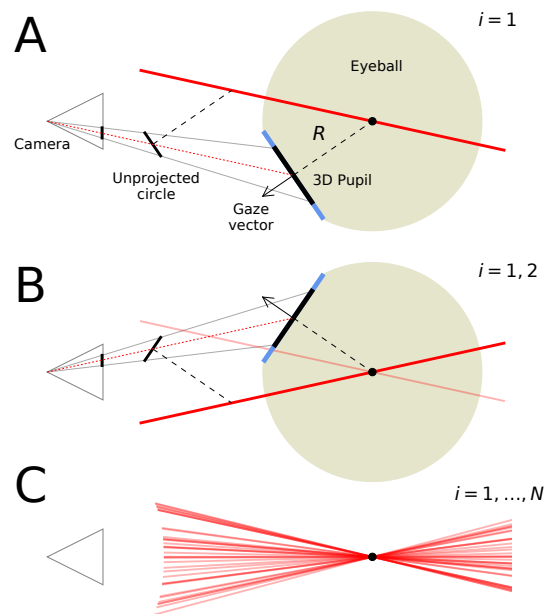
Figure 1: Estimating eyeball position by a least-squares intersection of lines. (A) Ignoring refraction effects occuring at corneal surfaces, the 3D circular pupil is mapped to a 2D ellipse in the image plane via perspective projection (shown in side view). After disambiguation, circular unprojections of the 2D pupil ellipse have a normal parallel to the gaze direction and their centers form a line passing through the center of the 3D pupil (dashed red line). Since the distance between eyeball and pupil center, R, is fixed, the eyeball center is constrained to lie on a parallel line (red solid line). (B) A change in gaze gives rise to an independent constraint for eyeball position. (C) Eyeball position is estimated by a least-squares intersection of constraining lines derived from a set of pupil contours.

environments. Remote eye trackers typically rely on complex optical setups involving the active generation of reflections by means of infrared (IR) LEDs and/or pairs of calibrated stereo cameras. Due to the technical infeasibility of robustly porting such solutions to head-mounted eye trackers, the latter need to solve the gaze-estimation problem with more restricted hardware setups. From an engineering point of view, glint-free gaze estimation using a single near-eye camera is highly desirable.

Recently, [Świrski and Dodgson 2013] have presented an approach for solving the gaze-estimation problem in this challenging setting. At its core, their method involves the time-intensive nonlinear optimization of a 3D eye model based on a set of pupil contours.

As demonstrated by [Dierkes et al. 2018], however, the approach by [Świrski and Dodgson 2013] suffers a severe limitation: by not accounting for corneal refraction it incurs systematic errors affecting eyeball-position, gaze-angle, and pupil-radius estimates. By reformulating eye-model optimization in terms of refraction-aware cost functions, [Dierkes et al. 2018] extended the approach and increased its optical veracity. While successfully accounting for refraction effects, their method comes at the cost of an increased conceptual and computational complexity.

Temporal integration of pupil-contour data, as in the approaches proposed by [Świrski and Dodgson 2013] and [Dierkes et al. 2018], is possible, since on short timescales the effects of headset slippage can be neglected. On timescales beyond several minutes, however, movements of head-mounted eye trackers with respect to the head of the user are unavoidable and need to be accounted for [Sugano and Bulling 2015]. One potential route for mitigating the effects of headset slippage is the real-time update of pertinent eye-model parameters based on recent observations. To enable such approaches, fast schemes for eye-model optimization need to be developed.

In this work we present a fast approach to refraction-aware eye-model fitting and gaze estimation that provides the same optical veracity as the one proposed by [Dierkes et al. 2018], albeit at a reduced conceptual and computational cost.

The specific contributions of this work are twofold. (i) We demonstrate that eye-model optimization can be recast as a least-squares intersection of lines. We furthermore present a method for estimating empirical refraction-correction functions which account for the systematic effects induced by corneal refraction. By means of a simulation study, we show that applying these correction functions leads to refraction-aware eyeball-position, gaze-angle, and pupil-radius estimates. (ii) Based on our novel approach, we present a statistical analysis of expected eyeball-position errors in the presence of pupil detection noise affecting real eye images. In particular, we quantify the beneficial effect of temporally integrating pupil contour information. Moreover, we present sensitivity functions which let us derive an estimate for the number of eye images required for enabling gaze-estimation with state-of-the-art accuracy.

2 RELATED WORK

Our work is related to previous studies on 1) model-based gazed estimation, especially 2) contour-based approaches and 3) work analyzing the repercussions of corneal refraction.

2.1 Model-based gaze estimation

Generally, video-based gaze-estimation methods can be categorized as being either regression- or model-based [Hansen and Ji 2010]. Recently, however, also learning-based approaches have been proposed [Mayberry et al. 2014; Tonsen et al. 2017]. Regression-based methods typically aim at predicting 2D gaze coordinates by means of phenomenological mapping functions [Fuhl et al. 2017, 2016; Javadi et al. 2015; Kassner et al. 2014; Mansouryar et al. 2016; Santini et al. 2018; Świrski et al. 2012; Tonsen et al. 2016]. Model-based

approaches, in contrast, perform gaze prediction based on a 3D eye model which is fit to features extracted from eye and/or face images. While the use of facial features has been explored [Chen and Ji 2008], typically pupil contours, pupil center position, and glints are used to infer 3D eye model parameters [Hansen and Ji 2010]. Here, we are concerned with a model-based approach using pupil contours alone.

2.2 Contour based approaches

Contour-based approaches analyze iris [Li and Li 2016; Tsukada and Kanade 2012; Tsukada et al. 2011; Wang et al. 2003] or pupil contours. Our approach is based on the analysis of pupil contours. [Li et al. 2018] employ an alternative cost-function compared to the one proposed by [Świrski and Dodgson 2013]. Their approach, however, necessitates an iterative minimization and in particular neglects the effects of refraction. A contour based approach dealing with refraction was developed by [Lai et al. 2015], but their method requires two cameras. Here, we are concerned with gaze estimation based on a single near-eye camera only.

2.3 Effects of corneal refraction

In a glint-based setting, refraction-effects have been accounted for by various approaches [Chen et al. 2008; Guestrin and Eizenman 2006; Hennessey et al. 2006; Ohno et al. 2002; Shih and Liu 2004]. All methods, however, rely on approximations of its nonlinear effects. The systematic errors in gaze-estimation accuracy incurred by ignoring/approximating refraction in a remote glint-based setting have been explored both experimentally and theoretically [Barsingerhorn et al. 2017; Villanueva and Cabeza 2008]. For head-mounted eye trackers which are based on pupil contours alone, such a study has been recently provided by [Dierkes et al. 2018]. The latter work also detailed a non-approximate approach for refraction-aware eye-model fitting and gaze estimation. The proposed method, however, necessitates two iterative optimizations, one for the eye model and one for gaze estimation. We show that refraction-aware eye-model fitting and gaze estimation is achievable in a non-iterative fashion and at a lower computational cost.

3 METHOD

In this section, after a brief review of the approach to eye-model fitting proposed by [Świrski and Dodgson 2013], we demonstrate that eye-model optimization can be recast in terms of a least-squares intersection of lines and thus lends itself to a non-iterative closed-form solution. Next, we detail how initial gaze estimation is performed based on an optimized eye model. We then go on to show that by making use of synthetic images, empirical refraction-correction functions can be estimated. These remedy the systematic errors introduced by ignoring corneal refraction which affects eyeball-position, gaze-angle, and pupil-radius estimates.

3.1 The Świrski model

The approach presented by [Świrski and Dodgson 2013] is based on the premise that 2D pupils as recorded by a near-eye camera are mere perspective projections of circular pupils, P, in 3D (see Fig. 1A). This constitutes a simplifying assumption since it neglects nonlinear distortions which are introduced to 2D pupil contours
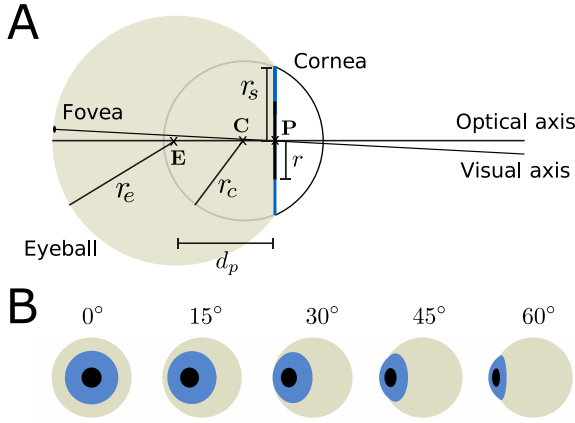
A

B

Figure 2: (A) Schematic of the two-sphere eye model according to LeGrand. (B) Examples of eye images generated by ray tracing of the two-sphere eye model with corneal refraction. Eyeball center $E = (0\,\text{mm}, 0\,\text{mm}, 35\,\text{mm})$; gaze angles as indicated. Adapted from [Dierkes et al. 2018].

by the effect of corneal refraction (see also [Aguirre 2018; Fedtke et al. 2010; Gehrmann and Atchison 2018]). 3D pupil circles, P, are modeled as being tangent to an eye sphere with radius R and center $E = (x, y, z)$. Here and in the following, all positions are defined with respect to a right-handed coordinate system coinciding with the center of the camera, which itself is facing along the positive z-axis. A 3D pupil $P = (\phi, \theta, r)$ is uniquely specified by its radius, r, and its position on the eye sphere in terms of spherical coordinates, ϕ and θ.

Given an eye image, a set of edges along the pupil contour is extracted by means of an automated pupil detection algorithm [Świrski et al. 2012]. Collecting pupil information over a period of time, thus results in N sets of two-dimensional pupil edges $\mathcal{E}_i = \{e_{ij} \text{ with } j = 1, \ldots, M_i\}$, where the subscript ranges over the number N of recorded images and M_i is the number of edges extracted from the i-th image. By means of an iterative optimization procedure, [Świrski and Dodgson 2013] estimate the parameters of a single sphere center E and N pupils $P_i = (\phi_i, \theta_i, r_i)$ that are consistent with the sets of pupil contours. Note, this approach assumes the eyeball to be stationary over the period pupil contours are collected.

In a first step, to each set of contour edges $\mathcal{E}_i$ an ellipse ℓ_i is fitted. Subsequently unprojecting ℓ_i, assuming a full perspective projection by a pinhole camera model and fixing an arbitrary positive radius r, results in two 3D circles [Safaee-Rad et al. 1992; Świrski and Dodgson 2013; Wang et al. 2003]. We will refer to these two circles as $v^r_{i,0}$ and $v^r_{i,1}$, their respective centers as $p^r_{i,0}$ and $p^r_{i,1}$, and their normals as $n_{i,0}$ and $n_{i,1}$. Note, the normals $n_{i,0}$ and $n_{i,1}$ do not depend on r.

In the following, we will denote by $\mathcal{T}$ the perspective projection that is associated with the camera and that is mapping points and vectors in 3D to the image plane. It is the case, that $\mathcal{T}(n_{i,0}) || \mathcal{T}(n_{i,1})$, i.e. after projection the two normals are parallel in image space. More specifically, one can show that the two lines $f_{i,0}(t) = \mathcal{T}(p^r_{i,0}) + t \cdot \mathcal{T}(n_{i,0})$ and $f_{i,1}(t) = \mathcal{T}(p^r_{i,1}) + t \cdot \mathcal{T}(n_{i,1})$ coincide. Furthermore,

they do not depend on r, since $\mathcal{T}(p^r_{i,0})$ and $\mathcal{T}(p^r_{i,1})$ are the same, respectively, for each choice of r. Each ellipse, ℓ_i, is thus associated with a unique line f_i in image space.

The intersection of all lines f_i coincides with $\overline{E} := \mathcal{T}(E)$, i.e. with the projection $\overline{E}$ of the eyeball center E. Due to noise and simplifying assumptions built into the model, the least-squares intersection of all lines f_i is taken as an estimate of the projected eyeball center.

Given $\overline{E}$, the two unprojected circles $v^r_{i,0}$ and $v^r_{i,1}$ can be disambiguated by noting that

$$\left\langle \mathcal{T}(n_{i,k}), \overline{E} - \mathcal{T}(p_{i,k}) \right\rangle > 0 \qquad (1)$$

for either $k = 0$ or $k = 1$, where $\langle ., . \rangle$ denotes the scalar product. In other words, the projected normal points away from the projected eyeball center for exactly one of the two unprojected circles. For each i, one chooses the respective circle, which we refer to as v^r_i, with center p^r_i and normal n_i.

Based on this disambiguation procedure, [Świrski and Dodgson 2013] derive a non-iterative algorithm for obtaining initial parameter estimates for E and all 3D pupils P_i. In a second step, a cost function depending on all parameters is then minimized, measuring the sum of suitable reprojection errors associated with all 3D pupils P_i. For details with respect to the initialization algorithm and the exact form of the cost function, we refer the reader to the original paper [Świrski and Dodgson 2013].

3.2 3D eye model

Our approach is based on the two-sphere eye model originally proposed by Le Grand [Le Grand 1957]. It approximates eye geometry as consisting of two partial spheres (see Figure 2). One sphere corresponds to the eyeball with center at position $E = (x, y, z)$ and radius of curvature r_e. The second sphere represents the corneal sphere with center C and radius of curvature r_c. We assume the cornea and aqueous humor to form a continuous medium with a single effective refractive index, n_{ref}. While the effective refractive index of the cornea varies slightly across the human population, we will for most of the following assume it to be fixed to the physiologically plausible value $n_{\text{ref}} = 1.3375$ [Guestrin and Eizenman 2006]. The iris and pupil, P, within the Le Grand eye model are two circles with radius r_s and r, respectively, sharing the same center, p, lying at a distance $d_p = \sqrt{r_e^2 - r_s^2}$ from E along the direction $\overline{EC}$. Their normals coincide, are parallel to $\overline{EC}$, and thus correspond to the optical axis of the eye. In the following, we will be concerned with estimating this optical axis of the eye.

The state of the model, similar to the one employed by [Świrski and Dodgson 2013], is uniquely determined by specifying the position of the eyeball center E and the pose and radius of the pupil $P = (\phi, \theta, r)$, where ϕ and θ are the spherical coordinates of the normalized vector pointing from E into the direction of C. Note, the radius R of the eye sphere in the Świrksi model is related to parameters in the Le Grand eye model via $R = d_p$. We will refer to ϕ and θ as gaze angles. In some cases, we will also refer to the angle between the optical axis and the negative z-axis as gaze angle. In order to assure that $\phi = \theta = 0$ corresponds to a zero gaze angle in the second sense, we adopt the following convention; given

Table 1: Eye model parameters used in the generation and analysis of synthetic and real eye images.

Parameter name	Symbol	Value	Reference
Eyeball radius	r_e	12 mm	[Bekerman et al. 2014]
Cornea radius	r_c	7.8 mm	[Guestrin and Eizenman 2006]
Iris radius	r_s	6.0 mm	[Gross 2008]
Pupil radius	r	1-4 mm	[Gross 2008]
Effective corneal refractive index	n_{ref}	1.3375	[Guestrin and Eizenman 2006]

the normalized gaze vector $(p - E)/\|p - E\|_2 = (\text{gv}_x, \text{gv}_y, \text{gv}_z)$, we define $(\phi, \theta) = (\arctan(\text{gv}_z/\text{gv}_x) + \pi/2, \arccos(\text{gv}_y) - \pi/2)$.

When not stated otherwise, the parameters in Table 1 were used. We generate synthetic images of the Le Grand eye model at 640x480 pixels resolution by means of a ray-tracing pipeline (see Figure 2B), in which we assume the camera to have a focal length of f=620 pixels. Refraction occuring at the air-cornea interface was implemented by means of Snell's law.

3.3 Non-iterative estimation of eyeball position

Optimization in the Świrksi framework results in both an estimate for eyeball position, E, as well as for gaze angles and pupil radii for all observations, given by $P_i = (\phi_i, \theta_i, r_i)$. Our approach, in contrast, proceeds in two stages. First, the eyeball center is determined. Gaze-angle and pupil-radius estimates are obtained in a separate step.

In order to determine eyeball position, we perform the same disambiguation procedure on pairs of unprojected circles as proposed by [Świrski and Dodgson 2013] (see Section 3.1). As a result, we obtain a set of circles v_i^r in 3D, corresponding to unprojections of fitted pupil contours ℓ_i.

We will now show that when fixing i, each unprojection v_i^r constrains the eyeball position in 3D to lie on a specific line (see Figure 1). To this end, note that for each choice of r, the circle v_i^r constitutes a 3D pupil candidate that is consistent with the observed pupil ellipse ℓ_i. In the framework of the two-sphere model, if v_i^r were to be the actual pupil, it would thus need to be tangent to a sphere of radius $R = d_p$ and position given by

$$g_i(r) = p_i^r - R \cdot n_i. \tag{2}$$

Note, Eq. (2) defines a line, g_i, in 3D that is parameterized by r. As the 3D pupil corresponds to v_i^r when r is chosen to be the actual pupil radius, the eyeball center E is indeed contained in g_i.

As any two different orientations of the optical axis give rise to corresponding g_i with linearly independent directions, eyeball position thus corresponds to the intersection of all g_i. Due to noise and simplifying assumptions built into the eye model, this intersection in practice needs to be taken in a least-squares sense. In closed-form it thus reads

$$E = \left(\sum_i I - d_i d_i^T\right)^{-1} \left(\sum_i \left(I - d_i d_i^T\right)(-Rn_i)\right), \tag{3}$$

where $d_i = p_i^r/\|p_i^r\|_2$ and $\|.\|_2$ denotes the usual Euclidean norm. By means of Eq. (3), eyeball position E can thus be determined in a non-iterative way.

3.4 Gaze estimation

After eyeball position, E, is estimated according to the method detailed in the last section, gaze estimation for additional eye images is performed in the following way. Given a fitted pupil contour, ℓ_i, an unprojected circle v_r^i is obtained for an arbitrary but fixed choice of r. Disambiguation is achieved by the criterion given in Eq. (1). Intersecting the line defined by the origin and p_i^r with a sphere at position E and radius $R = d_p$, provides an estimate for the center point of the pupil in 3D. The optical axis is given by the normalized direction from E to the intersection point. Pupil radius can be estimated by scaling the initial choice of r appropriately. Note, this method is implicitly contained in the initialization procedure by [Świrski and Dodgson 2013].

3.5 Correcting for refraction effects

As detailed in Sections 3.3 and 3.4, our proposed gaze-estimation approach proceeds in two stages. It has been shown previously [Dierkes et al. 2018] that by disregarding the effects of corneal refraction, both stages incur systematic errors. In this section, we present a method for estimating two empirical correction functions, $\mathcal{R}_{\text{eye}}$ and $\mathcal{R}_{\text{pupil}}$. These correction functions provide a fast and simple way to account for corneal refraction effects.

We will first detail our method with respect to correcting eyeball-position estimates. To this end, assume a set of eye images is given, with ground-truth eyeball position $E = (x, y, z)$. The estimate of E according to our proposed method in this section will be denoted by $\hat{E} = (\hat{x}, \hat{y}, \hat{z})$. While exhibiting systematic deviations from it, $\hat{E}$ depends on E in a bijective manner. We are seeking a correction function $\mathcal{R}_{\text{eye}}$ with the property that

$$\mathcal{R}_{\text{eye}}(\hat{E}, n_{\text{ref}}) = E, \tag{4}$$

for all eyeball positions E. Note, in Eq. (4) we have included n_{ref} as an independent parameter on the left hand side, as our correction function needs to be able to account for variations in the effective refractive index of the cornea across subjects. Due to the nonlinear nature of corneal refraction, the derivation of an exact closed-form representation of $\mathcal{R}_{\text{eye}}$ is challenging. Instead, we estimate $\mathcal{R}_{\text{eye}}$ in the following manner.

After fixing E at a position randomly drawn from a range of practically relevant eyeball positions, here $x, y \in [-5\,\text{mm}, 5\,\text{mm}]$ and $z \in [25\,\text{mm}, 45\,\text{mm}]$, we generated $N = 25$ synthetic eye images for a fixed value of n_{ref} randomly drawn from $[1.1, 1.4]$, with gaze angles ϕ and θ randomly chosen from a uniform distribution between $-50°$ and $50°$, and with pupil radii randomly chosen from a uniform distribution between 1 mm and 4 mm. Pupil contours were extracted from all images using Pupil Capture, the open source software developed by Pupil Labs [Kassner et al. 2014]. Based on the extracted contours, we obtained an eyeball position estimate $\hat{E}$ using the method detailed in Section 3.3. Repeating this procedure $M = 1000$ times resulted in a list of corresponding parameter tuples:

$$(\hat{x}_i, \hat{y}_i, \hat{z}_i, n_{\text{ref}}^i) \leftrightarrow (x_i, y_i, z_i) \quad \text{for } i = 1, \ldots, M.$$

We then estimated $\mathcal{R}_{\text{eye}}$ in a least-squares sense by means of a multivariate polynomial regression of degree $n = 5$. More specifically,

we defined

$$\mathcal{R}_{\text{eye}}(\hat{x}, \hat{y}, \hat{z}, n_{\text{ref}}) := \sum_{0 \le j, k, l, m, j+k+l+m \le 5} p_{j,k,l,m} \hat{x}^j \hat{y}^k \hat{z}^l n_{\text{ref}}^m, \quad (5)$$

for a set of parameters $P = \{p_{j,k,l,m} : 0 \le j, k, l, m, j+k+l+m \le 5\}$ which was minimizing the following sum of residuals:

$$\frac{2}{M} \sum_i \left\| \mathcal{R}_{\text{eye}}(\hat{x}_i, \hat{y}_i, \hat{z}_i, n_{\text{ref}}^i) - (x_i, y_i, z_i) \right\|^2. \quad (6)$$

We now turn to the estimation of the correction function $\mathcal{R}_{\text{pupil}}$, which is used to correct gaze-angle and pupil-radius estimates. More specifically, this requires the estimation of a function $\mathcal{R}_{\text{pupil}}$, such that

$$\mathcal{R}_{\text{pupil}}(E, \hat{\text{gv}}_x, \hat{\text{gv}}_y, \hat{\text{gv}}_z, \hat{r}, n_{\text{ref}}) = (\text{gv}_x, \text{gv}_y, \text{gv}_z, r),$$

for all eyeball positions E, gaze vectors gv, and pupil radii, r, where gaze-vector estimates are denoted by $\hat{\text{gv}}$ and estimated pupil radii are denoted by $\hat{r}$.

To this end, we fixed E and n_{ref} in a manner as detailed in the derivation of $\mathcal{R}_{\text{eye}}$. We then generated synthetic eye images on a grid of 20x20 images, with gaze vectors corresponding to gaze angles ϕ and θ evenly spanning a field of view of $-50°$ and $50°$, and pupil radii randomly chosen from a uniform distribution between 1 mm and 4 mm. For each image, we determined a gaze-vector, $\hat{\text{gv}}$, and pupil-radius estimate, $\hat{r}$, according to the method detailed in Section 3.4. Repeating this procedure M=1000 times resulted in a list of corresponding parameter tuples:

$$(E, \hat{\text{gv}}_x^i, \hat{\text{gv}}_y^i, \hat{\text{gv}}_z^i, \hat{r}_i, n_{\text{ref}}^i) \leftrightarrow (\text{gv}_x^i, \text{gv}_y^i, \text{gv}_z^i, r)$$

for $i = 1, \ldots, 400 \cdot M$. Given these data, we estimated $\mathcal{R}_{\text{pupil}}$ in a least-squares sense by means of a multivariate polynomial regression of degree $n = 5$, i.e. with a functional form and residuals being defined analogously to the ones given in Eq. (5) and Eq. (6), respectively.

In summary, given the two correction functions $\mathcal{R}_{\text{eye}}$ and $\mathcal{R}_{\text{pupil}}$, we propose the following two-stage gaze-estimation method. Based on a set of eye images, an uncorrected eyeball position $\hat{E}$ is determined according to Section 3.3, which after choosing an appropriate value for n_{ref}, can be corrected to a final estimate $E = \mathcal{R}_{\text{eye}}(\hat{E}, n_{\text{ref}})$. For subsequent frames, initial uncorrected estimates $\hat{\text{gv}}$ and $\hat{r}$ for gaze vector and pupil radius, respectively, are generated first according to Section 3.4. By means of the correction function $\mathcal{R}_{\text{pupil}}$, final estimates $(\text{gv}, r) = \mathcal{R}_{\text{pupil}}(E, \hat{\text{gv}}, \hat{r}, n_{\text{ref}})$ can then be determined.

4 EVALUATION

In this section, we report on a quantitative evaluation of the approach proposed in this work. Using both synthetic and real eye images, we present results gauging its performance with respect to eyeball-position, gaze-angle, and pupil-size estimation. In particular, we assess the effect of pupil detection noise, which is unavoidable for real eye imagery, and demonstrate the beneficial effect of temporally integrating pupil shape information.

4.1 Eyeball-position estimates

We first analyzed whether our approach is able to correctly extract eyeball positions from sets of synthetic eye images. To this
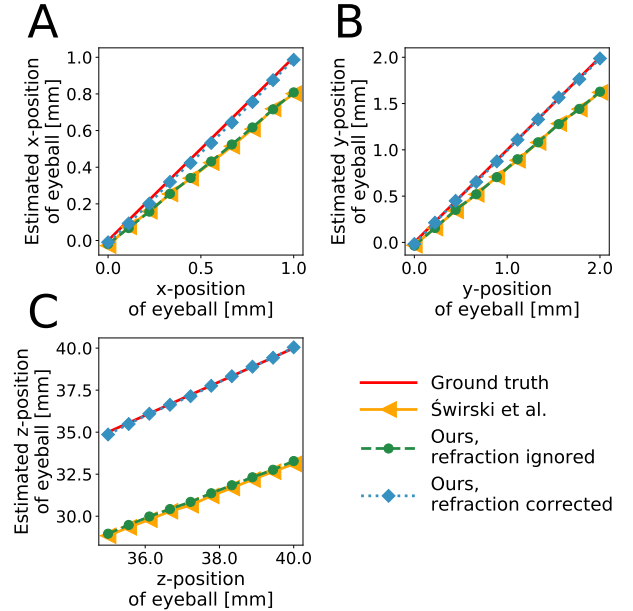

Figure 3: Estimates of eyeball position. (A-C) Estimated x-, y-, and z-position of the eyeball as a function of the respective ground truth value.

end, while keeping eyeball position fixed at a position E, we generated sets of N=25 synthetic eye images with gaze angles ϕ and θ randomly chosen from a uniform distribution between $-50°$ and $50°$. The pupil radius, r, for each image was chosen randomly from a uniform distribution between 1 mm and 4 mm. To mimic real eye images as close as possible, we set the refractive index of the cornea to $n_{\text{ref}} = 1.3375$ [Guestrin and Eizenman 2006]. Based on the extracted contours, we then optimized both Świrski's and our model. To the latter we furthermore applied our refraction correction function $\mathcal{R}_{\text{eye}}$. We repeated the above procedure for a series of eyeball positions E, covering a straight line connecting $E_0 = (0 \text{ mm}, 0 \text{ mm}, 35 \text{ mm})$ and $E_1 = (1 \text{ mm}, 2 \text{ mm}, 35 \text{ mm})$. The results of this analysis are shown in Figure 3.

As can be seen from the figure, Świrksi's and our model without correction lead to the same results in all cases (yellow and dashed green lines). As was shown previously [Dierkes et al. 2018], both approaches exhibit systematic deviations from ground truth values, as an effect of not taking into account corneal refraction. Applying our refraction correction function $\mathcal{R}_{\text{eye}}$, over the whole range of tested eyeball positions provides eyeball position estimates which are in very close agreement with ground truth values (dotted blue and red lines).

As a uniform distribution of pupil radii in a real-world setting cannot always be ensured, we next investigated the dependence of eyeball position estimates on pupil radius. To this end, we chose an eyeball position $E = (0 \text{ mm}, 0 \text{ mm}, z)$, varying z between 35 mm and 40 mm, and chose a pupil radius r, varying r between 1 mm and 4 mm. For each choice of E and r, we generated N=25 synthetic eye images with $n_{\text{ref}} = 1.3375$ and gaze angles ϕ and θ chosen from a uniform distribution between $-50°$ and $50°$. Based on
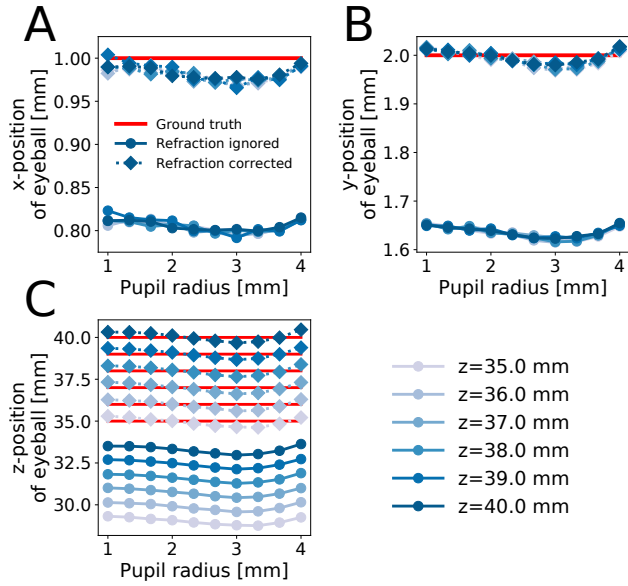
Figure 4: Estimates of eyeball position for fixed pupil radius. (A-C) Estimated x-, y-, and z-position of the eyeball as a function of ground truth value. Legend in (A) and lower right.
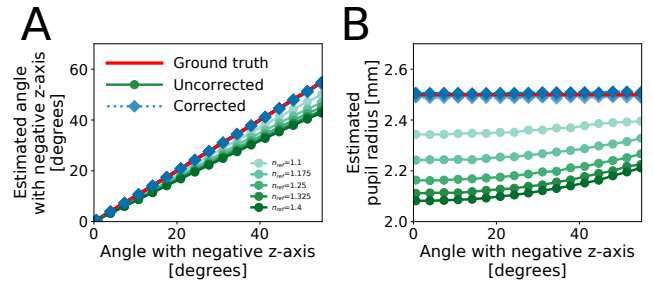

Figure 5: Accuracy of gaze-angle and pupil-radius estimates. (A) Uncorrected and corrected gaze-angle estimates. (B) Uncorrected and corrected pupil-size estimates. In both panels, estimates are shown as a function of the respective ground truth value for choices of the corneal refractive index, n_{ref}.

the extracted pupil contours, we optimized our model and applied the correction function $\mathcal{R}_{eye}$.

As can be seen from Figure 4, both the uncorrected and corrected eyeball-position estimates depend on pupil radius in a nonlinear fashion. In all cases, however, the observed variation is small, i.e. less than 2.5% as compared to the respective value observed for $r = 4\,mm$. More importantly, while the uncorrected estimates show systematic deviations from ground truth, the corrected estimates in all cases are close to ground truth values.

In summary, the results presented in this section attest that our approach successfully predicts eyeball positions from synthetic images. In particular, it successfully accounts for the effects of corneal refraction.

4.2 Angular gaze-estimation accuracy

Next, we quantified gaze-estimation accuracy. To this end, we clamped the eyeball at $E = (0\,mm, 0\,mm, 35\,mm)$, i.e. at a position frontal to the eye camera. We chose an effective refractive index of the cornea, n_{ref}, varying its value between 1.1 to 1.4. For each setting, we generated N=25 synthetic images, with gaze angles ϕ and θ being randomly chosen from a uniformly distribution between $-50°$ and $50°$. Pupil radius r was randomly chosen from a uniform distribution between 1 mm and 4 mm. Based on the extracted contours, we performed the non-iterative optimization of our model and applied the refraction correction function $\mathcal{R}_{eye}$. In a second step, we then generated synthetic eye images, varying gaze angle, as measured with respect to the negative z-axis, from $0°$ to $60°$ degrees and fixed the pupil radius at $r = 2.5\,mm$. For all images, we predicted the gaze angle and applied our refraction-correction function $\mathcal{R}_{pupil}$. In Figure 5A, we report the results of this analysis.

For $0°$ gaze angle and all choices of n_{ref}, all predictions (corrected and uncorrected) align with the ground truth value. For increasing gaze angle, however, uncorrected predictions exhibit a systematic error, which increases monotonically with gaze angle and refractive index. After correction, all predictions coincide with ground truth values up to line width.

These results show, that our approach faithfully captures the effect of refraction on gaze-angle estimates over a wide range of refractive indices.

4.3 Pupil-radius estimates

Next, we evaluated the accuracy of our approach with respect to pupil-radius estimates. To this end, we performed an analogous analysis to the one discussed in the previous section. This time, however, we obtained pupil radius estimates for all images. Our findings are summarized in Figure 5B.

For all choices of the corneal refractive index, n_{ref}, and all gaze angles tested, the uncorrected pupil-radius estimates are smaller than the ground truth value. This systematic error is maximal (about 25%) when the eye is looking directly at the camera and for the largest refractive index considered here. Furthermore, as was previously reported [Dierkes et al. 2018], uncorrected pupil-radius estimates vary with gaze angle. The observed variation is most pronounced for the largest refractive index tested. After application of our correction function $\mathcal{R}_{pupil}$, however, the obtained estimates match the ground truth values up to line width.

These result show that our method successfully produces correct pupil-radius estimates over a wide range of refractive indices.

4.4 Sensitivity to noise in real eye images

So far, we have considered synthetic eye images only. Pupil contours extracted from such synthetic eye images are perfect within pixel error and do not contain any noise. In a real-world setting, in contrast, gaze estimation has to be performed in the presence of such imperfections. In this section, we first quantify the importance of accurate eyeball position estimates for gaze estimation in terms of deterministic sensitivity functions. We then turn towards the analysis of real eye images and evaluate the performance of our approach in the presence of pupil contour noise.

Our method of gaze estimation depends on the prior determination of eyeball position. Errors in this position estimate directly translate to errors in subsequent gaze-angle estimates. In order to quantify the sensitivities χ_x, χ_y, and χ_z of the mean angular gaze-estimation error to imperfections in the x-, y-, and z-position of the eyeball, respectively, we performed the following analysis.

We generated synthetic eye images for an eye positioned directly in front of the camera at $E_0 = (0\,\text{mm}, 0\,\text{mm}, 35\,\text{mm})$ with $n_{\text{ref}} = 1.3375$ and pupil radius fixed at $r = 2\,\text{mm}$. Gaze angles ϕ and θ were chosen on a grid of 20x20 points, evenly spanning a field of view of $45°$ horizontally and vertically.

In a next step, we assumed an optimized eye model that was shifted away from the ground truth value, E_0, along one of the coordinate axis. More specifically, we chose $E_i(\Delta) = E_0 + \Delta * \vec{e}_i$, where $\Delta \in [-1.6\,\text{mm}, 1.6\,\text{mm}]$, $i \in x, y, z$, and $\vec{e}_i$ denotes the unit vector along the i-th coordinate axis. For each choice of E_i, we calculated corrected gaze-angle estimates for all images and determined the mean angular gaze-estimation error with respect to the ground truth.

As can be seen from the Figure 6A, shifts along each coordinate axis lead to a close to linear increase of the mean angular gaze-estimation error. Shifts along the x- and y-axis (orange and blue lines) effect a more pronounced increase as compared to shifts along the z-axis (green line). Due to symmetry, however, errors due to shifts along the x- and y-axis are almost identical. Taking the respective derivatives at $\Delta = 1$ mm, we can estimate the sensitivities $\chi_x \approx \chi_y \approx 5.80 \frac{\text{deg}}{\text{mm}}$ and $\chi_z \approx 1.45 \frac{\text{deg}}{\text{mm}}$. Thus errors in eyeball position estimates along the x- or y-axis lead to a mean angular gaze estimation error over the whole field of view that increases at about $5.80°$ per 1 mm shift. In the case of errors along the z-axis, sensitivity is lower, with the mean gaze estimation error growing at $1.45°$ per 1 mm shift. As a consequence, a necessary condition for achieving a mean angular gaze estimation error of below $1°$ is to be able to determine eyeball position with an error of less than 0.17 mm for the x- and y-axis and 0.68 mm for the z-axis.

We now turn to an analysis of real eye images. To this end, using the Pupil headset developed by Pupil Labs [Kassner et al. 2014], we generated recordings for $N = 6$ subjects each about 1 min in length. In order to mimic the setup of our simulation study, the eye camera of the headset was adjusted to face the eyeball centrally. Subjects were asked to evenly gaze in all directions for the full duration of the recording, thus approximately uniformly sampling their whole field of view. For each recording, pupil contours were extracted from all frames. Pupil contours as extracted by Pupil Capture are associated with a confidence value, C, gauging the overall quality of the contour and the likelihood of it not being a false detection. Only frames with $C > 0.98$ were kept, which corresponded to about 1500 frames per subject.

One of the challenges of working with real eye imagery is that no ground truth value for eyeball position is available. Due to noise in the extracted pupil contours, eyeball-position estimates in our approach vary with the exact choice of images that the optimization is based on. We thus performed a statistical analysis aimed at elucidating the expected error of our approach.

In Figure 6B, we show the distributions of x-, y-, and z-position estimates for a single subject, where the optimization was repeated
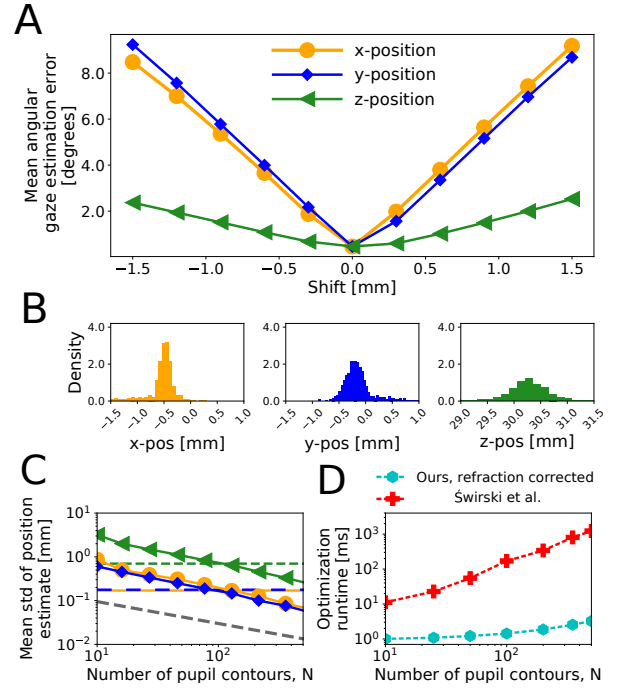

Figure 6: Effects of pupil contour noise. (A) Deterministic sensitivity functions. (B) Example densities of eyeball-position estimates ($N = 25$). (C) Mean standard deviation (n=6 subjects) of eyeball-position distributions as a function of the number of pupil contours, N, used for optimization. Colored dashed lines indicate thresholds for sub-1-degree gaze estimation as derived from A. Gray dashed line denotes a power law with exponent $\alpha = -1/2$. (D) Optimization runtimes as a function of the number of pupil contours, N, used for optimization. Color code for B, C in A.

1000 times based on $N = 25$ images that were randomly drawn from the full set of available frames. As can be seen from the figure, distributions are close to Gaussian and clearly centered around a mean value. Assuming the mean value to reflect the true position of the eyeball in the camera coordinate system, the standard deviation of the respective distributions thus serves as an estimate for the expected error in eyeball position estimates. For the data shown in Figure 6B, this corresponds to an error of 0.1 mm in x-, of 0.15 mm in y-, and of 0.34 mm in z-position.

To investigate whether using more pupil contours leads to a decrease in these error estimates, we determined the distributions shown in Figure 6B for choices of N between 10 and 500. We calculated their standard deviations and averaged them over different subjects.

The results are shown in Fig. 6C on a log-log-scale. We find that expected errors in x- and y-position are smaller than expected errors in z-position for all N. In all cases, errors decay with increasing N according to a power law with an exponent $\alpha = -1/2$ (see gray dashed line, which is proportional to $1/\sqrt{N}$). Note that the standard deviation of the sample mean of a normally distributed random variable follows the same pattern. Our results therefore

show that increasing the number of pupil contours in the optimization effectively averages out pupil contour noise, leading to ever decreasing expected errors on eyeball-position estimates. This demonstrates the positive effect of temporally integrating pupil contour information over the course of a recording.

Based on sensitivities χ_x, χ_y, and χ_z, and the results shown in Figure 6C, we can derive an explicit estimate for how many frames are needed for rendering the expected eyeball-position error low enough to facilitate a mean angular gaze-estimation error of less than one degree. We indicate the respective thresholds by colored dashed lines in 6C. We find that about 100 frames, corresponding to independent gaze directions, are sufficient to determine eyeball position with adequate accuracy.

While adding frames helps counteracting the detrimental effects of pupil contour noise, it comes at the cost of increased optimization runtimes. To compare the speed of our method with the one by [Świrski and Dodgson 2013], we measured mean runtimes as a function of the number of pupil contours, N, used during optimization. We employed the C++-implementation of the work by [Świrski and Dodgson 2013] as incorporated in Pupil Capture. Our novel approach was implemented in Python. Optimizations were run on a single core of an Intel(R) Core(TM) i7-6800K CPU @ 3.40GHz. Results are shown in Fig. 6D. For N=100, optimization with our approach takes about 1.5 ms. Optimization in the Świrski framework takes about two orders of magnitudes longer.

In summary, we have shown that by combining information drawn from a number of pupil contours our approach can overcome the limitations of unavoidable pupil contour noise and is expected to provide eyeball position estimates with high accuracy.

5 DISCUSSION

In this work, we proposed a fast non-iterative approach to refraction-aware 3D eye-model fitting and gaze prediction based on pupil contours alone. Leveraging geometrical insights with regard to the LeGrand two-sphere eye model, we cast the task of eyeball-position estimation as a least-squares intersection of lines. We accounted for systematic errors due to corneal refraction, both in eyeball-position and gaze and pupil-radius estimates, by means of empirical correction functions. In a simulation study we verified that our approach indeed provides accurate estimates for eyeball position, gaze angle, and pupil radius. Based on the statistical analysis of results obtained for real eye images, we showed the feasibility of our approach also in the presence of pupil contour noise. We demonstrated the beneficial effect of integrating pupil contour information over time. In particular, by combining our results with insights gleaned from deterministic sensitivity functions, we derived estimates for the number of independent eye images required to enable gaze estimation with a mean angular gaze-estimation error of one degree. While bearing similarities with the approach presented by [Świrski and Dodgson 2013] and [Dierkes et al. 2018], our method constitutes a considerable conceptual and computational simplification.

A key assumption made throughout this work is that the eyeball center is stationary in the camera coordinate system. So-called head-set slippage, i.e. unavoidable movements of the headset with respect to the head of the user, renders this assumption only approximately true. Indeed, headset slippage can occur on timescales

as short as minutes [Sugano and Bulling 2015] and constitutes a central challenge for head-mounted eye-tracking solutions. A promising route for mitigating the deteriorating effect of headset slippage is the continuous real-time update of eyeball position over the course of a recording. Such updates necessitate the repeated optimization of the eye model based on subsets of recent pupil contour observations. Earlier formulations of the eye-model optimization procedure, as e.g. presented in [Dierkes et al. 2018; Świrski and Dodgson 2013], involve time-intensive iterative solving of a non-linear minimization problem. Our approach, by being amenable to a fast non-iterative solution, considerably reduces the computational complexity and cost. It thus opens possibilities for devising more refined algorithms for detecting and correcting headset slippage. We showed that integrating pupil contour information over time renders eyeball-position estimates more accurate. By inducing shifts of the eyeball, headset-slippage, however, effectively limits the maximal integration time. One exciting route of investigation will be to quantify the time-scales associated with headset-slippage over a range of different activities. A statistical analysis of eyeball-position estimates obtained from subsets of the most recent eye images could then potentially be used to infer the current slippage-paradigm and inform strategies for real-time eye-model updates. We plan to explore these ideas in the future.

While we expect our work to facilitate progress in the development of glint-free head-mounted eye-tracking solutions, the current approach also faces certain limitations.

We demonstrated that it can successfully be used for the analysis of real eye images. The setup of our recordings, however, was highly controlled. In particular, by instructing subjects to gaze evenly within their field of view, the gaze-angle distributions obtained in our study were more uniform than in less controlled situations. It will be an interesting line of work to generalize the statistical estimates presented here to more realistic settings.

In this work, we have dealt with gaze estimation in a monocular setup only. As a consequence, the key metric used was angular gaze-estimation error as measured in the camera coordinate system. However, with the increasing pervasiveness of head-mounted displays in the field of AR/VR, the accurate estimation of gaze points in 3D becomes an increasingly important field of study [Elmadjian et al. 2018]. In particular, the effects of refraction in a binocular setting aimed at depth estimation have not been systematically explored. We believe our approach to provide a versatile and computationally accessible toolkit for addressing this exciting challenge.

6 CONCLUSION

In conclusion, we have presented a novel method for 3D eye model fitting and gaze estimation in a glint-free setting. Following our approach, eyeball position can be estimated from pupil contours alone by means of a least-squares intersection of lines. Systematic deviations introduced by corneal refraction are accounted for by means of empirical correction functions. The proposed method thus blends conceptual simplicity with a level of optical veracity which is necessary for achieving state-of-the-art gaze-estimation accuracy. We thus believe that it will serve as an accessible framework for tackling pressing challenges in the research and development of head-mounted eye-tracking solutions.

REFERENCES

G. K. Aguirre. 2018. A model of the entrance pupil of the human eye. *bioRxiv* (2018). https://doi.org/10.1101/325548

A. D. Barsingerhorn, F. N. Boonstra, and H. H. L. M. Goossens. 2017. Optics of the Human Cornea Influence the Accuracy of Stereo Eye-Tracking Methods: a Simulation Study. *Biomedical Optics Express* 8, 2 (2017), 712–725. https://doi.org/10.1364/BOE.8.000712

I. Bekerman, P. Gottlieb, and M. Vaiman. 2014. Variations in Eyeball Diameters of the Healthy Adults. *Journal of Ophthalmology* 2014, 3 (2014). https://doi.org/10.1155/2014/503645

J. Chen and Q. Ji. 2008. 3D Gaze Estimation With a Single Camera Without IR Illumination. In *ICPR 2008. 19th International Conference on Pattern Recognition.* IEEE, 1–4. https://doi.org/10.1109/ICPR.2008.4761343

J. Chen, Y. Tong, W. Gray, and Q. Ji. 2008. A Robust 3D Eye Gaze Tracking System Using Noise Reduction. In *Proceedings of the 2008 Symposium on Eye Tracking Research & Applications (ETRA '08).* ACM, New York, NY, USA, 189–196. https://doi.org/10.1145/1344471.1344518

K. Dierkes, M. Kassner, and A. Bulling. 2018. A novel approach to single camera, glint-free 3D eye model fitting including corneal refraction. *Proceedings of the 2018 ACM Symposium on Eye Tracking Research & Applications - ETRA '18* 9 (2018), 1–9. https://doi.org/10.1145/3204493.3204525

C. Elmadjian, A. D. Tula, and C.H. Morimoto. 2018. 3D gaze estimation in the scene volume with a head-mounted eye tracker. *COGAIN'18: Workshop on Communication by Gaze Interaction* (2018). https://doi.org/10.1145/3206343.3206351

C. Fedtke, F. Mann, and A. Ho. 2010. The Entrance Pupil of the Human Eye: a Three-Dimensional Model as a Function of Viewing Angle. *Optics Express* 18 (2010), 1–13. https://doi.org/10.1364/OE.18.022364

W. Fuhl, T. Santini, G. Kasneci, W. Rosenstiel, and E. Kasneci. 2017. PupilNet v2.0: Convolutional Neural Networks for CPU Based Real Time Robust Pupil Detection. *CoRR* (2017). https://arxiv.org/abs/1711.00112

W. Fuhl, M. Tonsen, A. Bulling, and E. Kasneci. 2016. Pupil detection for head-mounted eye tracking in the wild: An evaluation of the state of the art. *Springer Machine Vision and Applications* 27, 8 (2016), 1275–1288. https://doi.org/10.1007/s00138-016-0776-4

J. Gehrmann and D. A. Atchison. 2018. Pupil shape as viewed along the horizontal visual field Ankit Mathur. 13, 2013 (2018), 1–8. https://doi.org/10.1167/13.6.3.doi

H. Gross (Ed.). 2008. *Handbook of Optical Systems: Vol. 4 Survey of Optical Instruments.* Wiley-VCH Verlag GmbH+Co. KGaA, Weinheim.

E. D. Guestrin and M. Eizenman. 2006. General Theory of Remote Gaze Estimation Using the Pupil Center and Corneal Reflections. *IEEE Transactions on Biomedical Engineering* 53, 6 (2006), 1124–1133. https://doi.org/10.1109/TBME.2005.863952

D. W. Hansen and Q. Ji. 2010. In the Eye of the Beholder: A Survey of Models for Eyes and Gaze. *IEEE Transactions on Pattern Analysis and Machine Intelligence* 32, 3 (2010), 478–500. https://doi.org/10.1109/TPAMI.2009.30

C. Hennessey, B. Noureddin, and P. Lawrence. 2006. A Single Camera Eye-Gaze Tracking System With Free Head Motion. In *Proceedings of the 2006 Symposium on Eye Tracking Research & Applications (ETRA '06).* ACM, 87–94. https://doi.org/10.1145/1117309.1117349

A.-H. Javadi, Z. Hakimi, M. Barati, V. Walsh, and L. Tcheang. 2015. SET: a Pupil Detection Method Using Sinusoidal Approximation. *Frontiers in Neuroengineering* 8 (2015). https://doi.org/10.3389/fneng.2015.00004

M. Kassner, W. Patera, and A. Bulling. 2014. Pupil: an Open Source Platform for Pervasive Eye Tracking and Mobile Gaze-Based Interaction. In *Proceedings of the 2014 ACM International Joint Conference on Pervasive and Ubiquitous Computing: Adjunct Publication.* ACM, 1151–1160. https://doi.org/10.1145/2638728.2641695

C.-C. Lai, S.-W. Shih, and Y.-P. Hung. 2015. Hybrid Method for 3-D Gaze Tracking Using Glint and Contour Features. *IEEE Transactions on Circuits and Systems for Video Technology* 25, 1 (2015), 24–37. https://doi.org/10.1109/TCSVT.2014.2329362

Y. Le Grand. 1957. *Light, Color and Vision.* Wiley, New York, NY, USA.

J. Li and S. Li. 2016. Two phase approach - Calibration and iris contour estimation - For gaze tracking of head-mounted eye camera. *2016 IEEE International Conference on Image Processing (ICIP)* (2016), 3136–3140. https://doi.org/10.1109/ICIP.2016.7532937

J. Li, S. Li, T. Chen, and Y. Liu. 2018. A Geometry-Appearance-Based Pupil Detection Method for Near-Infrared Head-Mounted Cameras. *IEEE Access* 6 (2018), 23242–23252. https://doi.org/10.1109/ACCESS.2018.2828400

M. Mansouryar, J. Steil, Y. Sugano, and A. Bulling. 2016. 3D Gaze Estimation from 2D Pupil Positions on Monocular Head-Mounted Eye Trackers. In *Proc. of the 9th ACM International Symposium on Eye Tracking Research & Applications (ETRA).* 197–200. https://doi.org/10.1145/2857491.2857530

A. Mayberry, P. Hu, B. Marlin, C. Salthouse, and D. Ganesan. 2014. iShadow: Design of a Wearable, Real-time Mobile Gaze Tracker. In *Proceedings of the 12th Annual International Conference on Mobile Systems, Applications, and Services.* 82–94. https://doi.org/10.1145/2594368.2594388

T. Ohno, N. Mukawa, and A. Yoshikawa. 2002. FreeGaze: A Gaze Tracking System for Everyday Gaze Interaction. *Proceedings of the 2002 Symposium on Eye Tracking Research & Applications (ETRA '02)* (2002), 1–8. https://doi.org/10.1145/507072.507098

R. Safaee-Rad, I. Tchoukanov, K. C. Smith, and B. Banhabib. 1992. Three-Dimensional Location Estimation of Circular Features for Machine Vision. *IEEE Transactions on Robotics and Automation* 8, 5 (1992), 624–640. https://doi.org/10.1109/70.163786

T. Santini, W. Fuhl, and E. Kasneci. 2018. PuRe: Robust Pupil Detection for Real-Time Pervasive Eye Tracking. *Computer Vision and Image Understanding* (2018). https://doi.org/10.1016/j.cviu.2018.02.002

S. W. Shih and J. Liu. 2004. A Novel Approach to 3-D Gaze Tracking Using Stereo Cameras. *IEEE Transactions on Systems, Man and Cybernetics, Part B (Cybernetics)* 34, 1 (2004), 234–245. https://doi.org/10.1109/TSMCB.2003.811128

Y. Sugano and A. Bulling. 2015. Self-calibrating Head-mounted Eye Trackers Using Egocentric Visual Saliency. In *Proceedings of the 28th Annual ACM Symposium on User Interface Software & Technology (UIST).* 363–372. https://doi.org/10.1145/2807442.2807445

L. Świrski, A. Bulling, and N. Dodgson. 2012. Robust Real-Time Pupil Tracking in Highly Off-Axis Images. In *Proceedings of the Symposium on Eye Tracking Research & Applications (ETRA '12).* 173–176. https://doi.org/10.1145/2168556.2168585

L. Świrski and N. A. Dodgson. 2013. A Fully-Automatic, Temporal Approach to Single Camera, Glint-Free 3D Eye Model Fitting. In *Proceedings of ECEM 2013.* http://www.cl.cam.ac.uk/research/rainbow/projects/eyemodelfit/

M. Tonsen, J. Steil, Y. Sugano, and A. Bulling. 2017. InvisibleEye: Mobile Eye Tracking Using Multiple Low-Resolution Cameras and Learning-Based Gaze Estimation. *Proceedings of the ACM on Interactive, Mobile, Wearable and Ubiquitous Technologies (IMWUT)* (2017). https://doi.org/10.1145/3130971

M. Tonsen, X. Zhang, Y. Sugano, and A. Bulling. 2016. Labelled pupils in the wild: A dataset for studying pupil detection in unconstrained environments. In *Proc. of the 9th ACM International Symposium on Eye Tracking Research & Applications (ETRA).* 139–142. https://doi.org/10.1145/2857491.2857520

A. Tsukada and T. Kanade. 2012. Automatic Acquisition of a 3D Eye Model for a Wearable First-Person Vision Device. In *Proceedings of the Symposium on Eye Tracking Research & Applications (ETRA '12).* https://doi.org/10.1145/2168556.2168597

A. Tsukada, M. Shino, M. Devyver, and T. Kanade. 2011. Illumination-Free Gaze Estimation Method for First-Person Vision Wearable Device. *IEEE International Conference on Computer Vision Workshops* (Nov. 2011), 2085–2091. https://doi.org/10.1109/ICCVW.2011.6130505

A. Villanueva and R. Cabeza. 2008. Evaluation of Corneal Refraction in a Model of a Gaze Tracking System. *IEEE Transactions on Biomedical Engineering* 55, 12 (2008), 2812–2822. https://doi.org/10.1109/TBME.2008.2002152

J.-G. Wang, E. Sung, and R. Venkateswarlu. 2003. Eye Gaze Estimation from a Single Image of One Eye. *Proceedings of the Ninth IEEE International Conference on Computer Vision (ICCV)* (2003), 1–8. https://doi.org/10.1109/ICCV.2003.1238328